IEEE Access
Multidisciplinary | Rapid Review | Open Access Journal

Received 16 July 2024, accepted 13 August 2024, date of publication 20 August 2024, date of current version 2 September 2024.

Digital Object Identifier 10.1109/ACCESS.2024.3446691

RESEARCH ARTICLE

A Multi-Mode Superposition Technique for Circular Polarized Beamforming and Steering in Mobile Communication and Radar Systems

FATEMEH AKBAR[1], (Member, IEEE), AND BEHZAD YEKTAKHAH[2], (Member, IEEE)
[1]Department of Electrical Engineering, Sharif University of Technology, Tehran 1458889694, Iran
[2]Department of Electrical Engineering and Computer Science, University of Michigan, Ann Arbor, MI 48109, USA

Corresponding author: Fatemeh Akbar (fakbar@sharif.edu)

ABSTRACT Focusing electromagnetic energy into a narrow sliver of space (beamforming) and directing this energy to desired areas (beam steering), which have been conventionally achieved using phased array antennas, allow for mitigating the propagation loss of energy and are critical for emerging communication and radar systems. This work presents a novel beamforming and steering technique which is based on the superposition of circular waveguide transverse electric (TE_{n1}) modes. In this technique, a plurality of superposed omnidirectional circular polarized (CP) TE_{n1} waves, where each wave has a specific azimuthal radiation phase profile, is created. The unique phase profile of each wave is leveraged for CP beamforming and 360° beam steering. The proposed beamforming and steering approach can be realized using a single antenna structure with a relatively small dimension. It can be integrated into user mobile equipment, vehicles, base stations, repeaters, and radars, and due to its CP radiation, would be more immune to multipath fading and multiple reflections. It can also eliminate the requirement of a precise alignment for transmitting and receiving antennas. A CP beamformer antenna performing based on the proposed method is designed and fabricated for operation within 26.5-29.5 GHz which covers n257 and n261 bands for 5G systems. The test results verify the functionality of the proposed CP beamforming and steering technique. This technique can also be adapted for high-resolution automotive radars by employing a rotating antenna, and preliminary simulation and measurement results are also presented.

INDEX TERMS 5G, automotive, beam steering, beamforming, circular polarization, phased array, radar, repeater, user equipment.

I. INTRODUCTION

Emerging radar and communication technologies take advantage of the wide spectrum available at millimeter-wave (mm-wave) frequencies to enable high resolution detection and high throughput communications, respectively. Fifth generation (5G) wireless technology, operating within the mm-wave band with low latency, facilitates advanced applications such as Internet-of-Things (IoT) and Vehicle-to-Everything (V2X) communication [1], [2], [3]. V2X enhances automotive and traffic safety by enabling collaboration and data exchange among the elements in the traffic environment.

Despite benefiting from a larger available bandwidth, as compared to the few gigahertz RF frequencies, communication systems at mm-wave frequencies, such as 5G, suffer more from penetration loss (losses caused by wave propagation through buildings and walls), attenuation caused by rain and foliage, diffraction, and shadowing effect caused by obstacles. Mm-wave wireless operation would also be more adversely impacted by the fading effect due to the increased interactions with the surrounding environment specifically in the crowded urban areas [4], [5]. Therefore, a single omnidirectional antenna radiating energy in all directions

The associate editor coordinating the review of this manuscript and approving it for publication was Debabrata K. Karmokar.

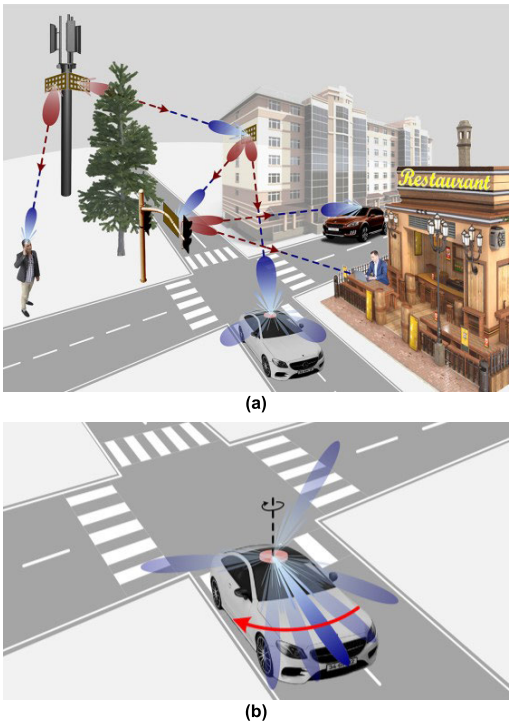

FIGURE 1. (a) Multiple repeaters with beamforming and steering capability in mm-wave communication systems, such as 5G and V2X, to enable bouncing the signals around blocking obstacles and directing the power to the desired areas. Proposed antenna can be mounted on the vehicle roof for beamforming and 360° beam steering in 5G communications. (b) Proposed rotating antenna can be mounted on the vehicle roof for high angular resolution beamforming and 360° beam steering in automotive radar applications.

would not work well in case of mm-wave communications. Instead, as illustrated in Fig. 1(a), the energy emission should be directed to the desired areas and bounced around blocking obstacles [6]. Thus, beamforming and steering are required in base stations, repeaters, user equipment (UE), and radars. For mobile UEs, such as cars in 5G V2X networks and 5G mobile handheld devices, the beamforming and steering systems should provide full 360° coverage in azimuth.

In addition to spatial selectivity, the emerging radar and communication technologies also require circular polarized (CP) radiation for enhanced performance [6]. In radar applications, CP increases the isolation between the transmitter and receiver, reduces the effect of multiple reflections (appearing as clutter in radar output), and enables detection/imaging of targets with large aspect ratios or arbitrary orientations. In communication systems, CP radiation suffers less from multi-path fading and polarization mismatch loss between transmitting and receiving antennas. CP radiation also eliminates the requirement of a precise alignment between transmitting and receiving antennas which is particularly important for satellite communications (where Faraday rotation affects the polarization angle of linear polarized waves as they pass through ionosphere and causes misalignment between linear polarized antennas) [7].

All these requirements mean that a need exists for beam formation and steering with circular polarization over a wide or 360° range. Several designs are available for linear polarized and CP linear arrays for satellite communications and 5G mobile terminals (including vehicles); however, such designs have a limited beam steering range and do not provide 360° coverage [8], [9], [10], [11], [12], [13], [14], [15]. To provide a wide beam steering range for 5G mobile terminals, [16] has proposed an antenna array consisting of multiple CP linear arrays that face different directions. However, this design is not compact, and its lateral dimension is more than $5\lambda_0 \times 11\lambda_0$ (where λ_0 is the wavelength at the center frequency of operation). Several designs have been proposed for full azimuthal coverage using multiple linearly polarized antennas oriented in different directions. These designs, however, are large in both diameter and height relative to the wavelength [17], [18].

A novel CP beamforming and steering approach that can be realized using a low-profile antenna was presented in [19]. In this method, a CP conical beam (a radiation pattern which is omnidirectional over azimuth and directional over elevation) is created by exciting degenerate circular (waveguide) transverse electric (TE_{n1}) modes. To provide spatial selectivity, a plurality of superposed omnidirectional circular TE_{n1} waves, where each wave has a unique azimuthal radiation phase profile, are excited. The distinctive phase profile of these waves is leveraged for beamforming and steering over 360° of azimuth. This paper extends the work in [19] by i) elaborating on the operation principle of the new beamforming and steering method, ii) analyzing its detailed performance, iii) developing an antenna structure that realizes the proposed CP beamforming and steering technique, and iv) introducing a method to synthesize the proposed CP beamforming and steering technique for high angular resolution using a rotating antenna. Furthermore, it presents detailed simulation and measurement results, verifying the functionality and advantages of the introduced methods. The key advantages of the described beamforming and steering technique and its realizing antenna are (a) providing 360° CP beam steering using a single, low-profile, compact antenna, which makes the described design suitable for integration with UE; (b) compatibility of the antenna structure with integrated circuit technology, allowing for an on-chip design; (c) the ability to easily switch the antenna's CP radiation pattern between an omnidirectional pattern and a steerable directional pattern by changing only the phases and amplitudes of the excitations, and (d) the capability of achieving a very high angular resolution for radar and imaging applications by synthesizing the method using a simple rotating antenna.

The proposed beamforming and steering antenna is designed to operate within 26.5-29.5 GHz for 5G mobile systems (covering both n257 and n261 bands). It has a diameter of $2.43\lambda_0$ and a height of $0.26\lambda_0$ (excluding the connector), and with such a small size, can be integrated to UE as well as other nodes such as repeaters. Unlike the designs with multiple planar arrays facing different directions, radiation pattern characteristics of the proposed antenna are maintained as its beam is steered over azimuth. The same performance

could be achieved using a circular array of omnidirectional CP antennas. However, large size of such antennas [20], [21], [22], [23] (typically larger than $0.5\lambda_0 \times 0.5\lambda_0$) and the requirement of a certain spacing between them to control their coupling, necessitates a careful design to avoid the occurrence of grating lobes.

With features such as a low profile, small size, 360° beam steering range with CP radiation, and directive end-fire pattern, the antenna emerges as an ideal candidate for various applications. For instance, it is well-suited for 5G and beyond communication in mobile devices and vehicles [24], [25]. As shown in Fig. 1(a), it can be mounted on the roof of a vehicle to provide comprehensive 360° coverage. Furthermore, the antenna's planar structure and feed design make it suitable for on-chip integration at higher frequency bands.

This paper also explores the application of the proposed CP beamforming and steering method in high-resolution radar systems with full coverage. In surveillance and automotive radar applications, it is imperative to achieve 360° coverage of the radar system with high angular resolution. In automotive scenarios, this is typically accomplished by employing either mechanically or electronically scanning LIDARs, or multiple mm-wave phased array radars (each scanning limited areas) mounted on different parts of a vehicle and oriented in different directions. LIDAR systems offer high angular resolution and full coverage, but their performance suffers in adverse weather conditions. In contrast, mm-wave radars can operate in severe weather conditions like fog, rain, snow, and dust; however, they provide less coverage and lower angular resolution compared to LIDARs [26]. This paper demonstrates that by synthetically realizing the proposed method using a simple rotating antenna, it is possible to obtain the advantages of both LIDARs (high resolution with low complexity) and mm-wave phased array radars (functionality in severe weather conditions). Preliminary simulation and measurement results show that a very narrow 360° steerable CP beam can be achieved using a small antenna, unlike conventional antenna arrays that typically require larger sizes. This method finds specific applications in automotive radar systems with complete 360° coverage, as illustrated in Fig. 1(b) (antenna mounted on the roof).

The paper is organized as follows. Section II discusses the generation of an omnidirectional CP radiation by exciting a TE_{n1} mode and its rotated copy. Section III demonstrates the provision of spatial selectivity through the excitation of multiple TE_{n1} modes and their rotated copies and includes a method for its realization. Section IV presents an antenna structure designed to implement the proposed beamforming and steering method. The simulation and measurement results of the fabricated antenna are discussed in Section V. Section VI includes the synthesis of the proposed method, aimed at providing a very narrow beam for high-angular-resolution 360° radar coverage and presents preliminary simulated and measured results. Concluding remarks are given in Section VII.

II. CP OMNIDIRECTIONAL RADIATION

A. CIRCULAR TE_{n1} MODES

For a circular (waveguide) TE_{n1} mode excited within a circular aperture with the radius of a (shown in Fig. 2(a)), the electric field ($\bar{E}_n$) is given by

$$\bar{E}_n = \frac{n}{\rho} J_n\left(\frac{\chi'_{n1}}{a}\rho\right) \sin(n\phi)\,\hat{\rho} + \frac{\chi'_{n1}}{a} J'_n\left(\frac{\chi'_{n1}}{a}\rho\right)\cos(n\phi)\,\hat{\phi}, \quad (1)$$

where ρ and ϕ define a position on the aperture in the cylindrical coordinate system. In (1), J_n is the Bessel function of the first kind and nth order, J'_n denotes the derivative of J_n, and χ'_{n1} is the first zero of J'_n which is equal to 1.841, 3.054, 4.201, and 5.317 for the first four modes ($n = 1$, 2, 3, and 4), respectively.

It is proved in [19] that the farfield electric field ($\bar{E}_{ff,n}$) radiation of the TE_{n1} mode excited within the aperture can be written as

$$\bar{E}_{ff,n}(\phi) = A_\theta(n,\theta)\sin(n\phi)\,\hat{\theta} + A_\phi(n,\theta)\cos(n\phi)\,\hat{\phi}. \quad (2)$$

where A_θ and A_ϕ are functions of mode number (n) and θ. According to (2), the farfield radiation has the following characteristics

- Radiation is linear polarized at each azimuthal angle.
- Polarization tilt angle varies with ϕ, and its variation rate increases with mode number (n).
- Linear polarizations are orthogonal at the locations with angular spacing of $180°/(2n)$.

These characteristics are verified for $n = 2$ in Fig. 2(b) (representing the farfield electric field due to the TE_{21} mode excited within the aperture).

B. EXCITATION OF A TE_{n1} MODE AND ITS ROTATED COPY

Considering that the linear polarized radiations generated by TE_{n1} modes are orthogonal at azimuthal locations with angular spacing of $180°/(2n)$, exciting two TE_{n1} modes with a relative azimuth angle of $180°/(2n)$ results in two orthogonal linear polarized field components at each ϕ. In this case, a CP radiation will be obtained if the two modes are excited with the same amplitude and a relative phase of 90°, which has been fulfilled in this work. The resulting total farfield electric field would equal

$$\bar{E}_{ff,tot}(\phi) = \bar{E}_{ff,n}(\phi) + e^{-j\frac{\pi}{2}}\bar{E}_{ff,n}\left(\phi - \frac{\pi}{2n}\right) = A_\theta(\sin(n\phi) + j\cos(n\phi))\,\hat{\theta} + A_\phi(\cos(n\phi) - j\sin(n\phi))\,\hat{\phi}. \quad (3)$$

Taking the criteria of axial ratio (AR) < 3 dB (for a decent CP radiation) into account, (3) indicates a right-handed CP (RHCP) radiation if $|A_\theta/A_\phi|$ falls within the ±3-dB range. A left-handed CP (LHCP) radiation can also be obtained by an excitation phase of +90° for the rotated mode in (3). The ratio $|A_\theta/A_\phi|$ is plotted in Fig. 3 for different modes (n) and aperture radii (a). It can be observed that the range of θ associated with a CP radiation is a function of mode number and a/λ_0.

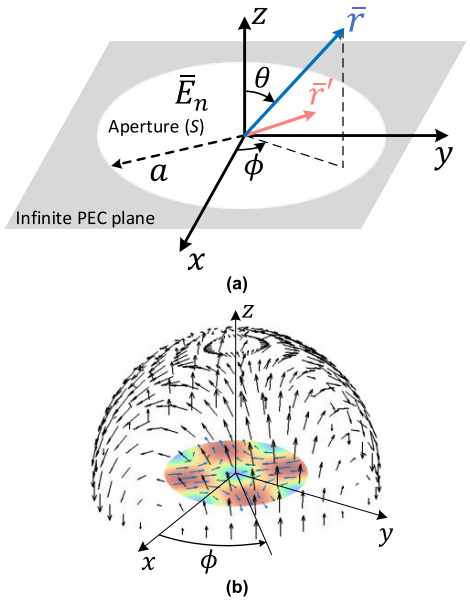

FIGURE 2. (a) Circular aperture with a radius of a. (b) Farfield electric field vectors due to the TE_{21} mode excited within the aperture with radius $a = 0.5\ \lambda_0$.

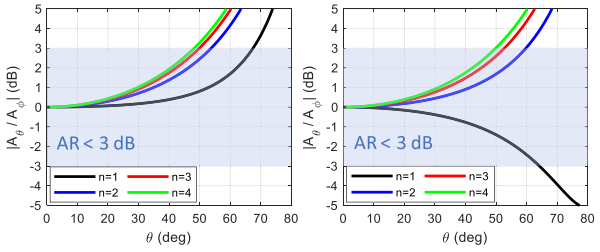

FIGURE 3. $|A_\theta/A_\phi|$ versus θ for different TE_{n1} modes. (a) $a/\lambda_0 = 0.5$. (b) $a/\lambda_0 = 0.6$.

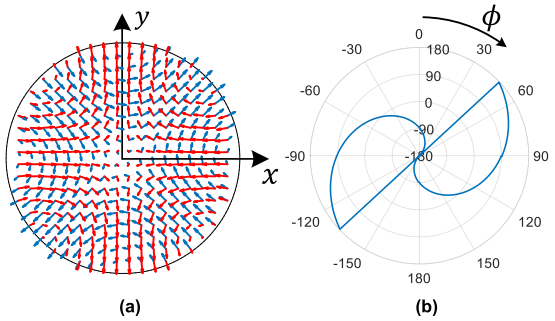

FIGURE 4. (a) TE_{21} mode and its rotated copy for generating omnidirectional CP radiation. (b) Azimuthal phase profile (ϕ is defined in Fig. 2(a)) of the omnidirectional CP radiation obtained by TE_{21} mode and its rotated copy.

Figure 4(a) shows TE_{21} mode and its rotated copy for generating omnidirectional CP radiation.

III. BEAMFORMING AND STEERING

A. SPATIAL SELECTIVITY THROUGH THE EXCITATION OF MULTIPLE TE_{n1} MODES AND THEIR ROTATED COPIES

Assuming a CP antenna with the same handedness exists on the receiver side, it can be shown (by reciprocity) that the received signal due to the radiation described by (3) would be equal to $Ae^{-jn\phi}$ where A is a constant. This indicates that at a fixed radial distance from the transmitter, phase of the radiated CP fields varies by $n\phi$. Figure 4(b) shows azimuthal phase profile (phase over ϕ) of the radiated CP fields at a fixed r and $\theta = 60°$ for TE_{21} mode and its rotated copy. It can be observed that the phase varies by 2ϕ as ϕ varies within 0-360°.

If the first N TE_{n1} modes ($n = 1, 2, \ldots, N$) in conjunction with their rotated copies are excited, then the amplitude of the total farfield radiation is given by

$$S = \left| A \sum_{n=1}^{N} e^{-jn\phi} \right| = \left| A \frac{\sin\left(\frac{N\phi}{2}\right)}{\sin\left(\frac{\phi}{2}\right)} \right|, \tag{4}$$

where A is a constant. The summation in (4) shows a directive pattern with the main beam at $\phi = 0°$. To enable beam steering, a phase of $n\phi_s$ should be added to the nth mode and its rotated copy. The resulting farfield radiation would be

$$S = \left| A \sum_{n=1}^{N} e^{-jn(\phi-\phi_s)} \right| = \left| A \frac{\sin\left(\frac{N(\phi-\phi_s)}{2}\right)}{\sin\left(\frac{\phi-\phi_s}{2}\right)} \right|. \tag{5}$$

Equation (5) indicates a directive pattern with the main beam steered to $\phi = \phi_s$, where ϕ_s can vary within 0-360°. In fact, each TE_{n1} mode in conjunction with its rotated copy acts like an antenna element in a conventional phased array. However, here, the pattern shape does not change with steering direction. By adjusting the excitation amplitude of each TE_{n1} mode and its rotated copy, the radiation pattern can be shaped and its parameters like 3-dB beamwidth and side lobe levels can be controlled.

B. A METHOD FOR EXCITING MULTIPLE TE_{n1} MODES AND THEIR ROTATED COPIES

According to (1), the electric field of a TE_{n1} mode is purely radial at $2n$ equally separated azimuthal angles within 0-360°. Considering that a radial current can produce a significant radial electric field, one can excite $2n$ radial electric currents with an equal angular spacing to generate a TE_{n1} mode. To excite the rotated copy of the TE_{n1} mode, another set of $2n$ radial currents with a relative azimuthal angle of $180°/(2n)$, a relative excitation phase of 90°, and the same amplitude as the first set is also used. Thus, to excite the nth mode and its rotated one, $2(2n)$ radial currents are needed, and the required excitation amplitude and phase for the mth current ($m = 1, 2, \ldots, 4n$) is $1\angle(90° \times (m-1))$. Figure 5(a) shows the currents required for exciting TE_{21} mode and its rotated copy to provide a CP omnidirectional radiation.

To excite the entire first N TE_{n1} modes ($n = 1, 2, \ldots, N$) along with their rotated copies for beamforming and steering purposes, $2(2N)$ radial currents are needed. Within such architecture, the required excitation amplitude and phase for the mth current ($m = 1, 2, \ldots, 4N$) to excite the nth ($n = 1, 2, \ldots, N$) mode is

$$I_m = 1e^{-j\left(\frac{2\pi}{4N}n(m-1)\right)}. \tag{6}$$

Thus, to uniformly excite the entire first N TE_{n1} modes and their rotated copies and to steer the main beam to $\phi = 0°$, the

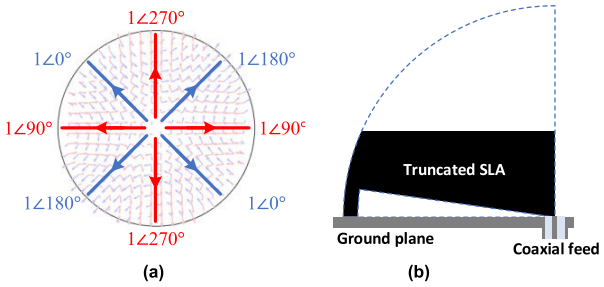

FIGURE 5. (a) Radial currents required for excitation of a TE_{21} mode in conjunction with its rotated copy. (b) Original structure (dashed line) and truncated structure for a monopole SLA element on the ground plane with a coaxial feed.

required excitation signal at mth element (I_m) is

$$I_m = \sum_{n=1}^{N} 1e^{-j\left(\frac{2\pi}{4N}n(m-1)\right)}. \tag{7}$$

Equation (7) assumes that the fields radiated by all modes are the same in amplitude and phase at $\phi = 0°$ and $\theta = \theta_s$, where θ_s is the main beam direction in elevation. However, in an antenna realizing the described beamforming and steering method, the phases and amplitudes of the different modes are not necessarily the same at $\phi = 0°$ and $\theta = \theta_s$. The difference in their radiation phase and amplitude can be compensated by complex coefficients in excitation. In general, for beamforming and steering purposes, I_m should be

$$I_m = \sum_{n=1}^{N} a_n c_n e^{-j\left(\frac{2\pi}{4N}n(m-1)-n\phi_s\right)}, \tag{8}$$

where ϕ_s is the beam steering angle (within 0°-360°), a_n is the amplitude scaling (tapering) factor of the nth mode for pattern shaping purposes, and c_n is the complex compensation coefficients defined as

$$c_n = \frac{1}{\sqrt{G_{realized,n}(\theta = \theta_s, \phi = 0°)}e^{jP_n(\theta=\theta_s,\phi=0°)}}. \tag{9}$$

In (9), $G_{realized,n}(\theta = \theta_s, \phi = 0°)$ and $P_n(\theta = \theta_s, \phi = 0°)$ are the absolute value of realized CP gain and phase (in radian) of the radiated CP electric field, respectively, for the nth mode at $\phi = 0°$ and $\theta = \theta_s$.

To operate within a wide frequency band, the required radial currents must be generated by wideband structures. Monopole sectorial loop antennas (SLA) [27], can be used for this purpose. The original design for a monopole SLA is shown in Fig. 5(b) by dashed lines. It consists of a sector on a ground plane which is short-circuited at the end by an arc. The SLA is radially placed on the ground plane and is fed by a coaxial probe. The magnetic field created by the SLA loop compensates for the input capacitance, and as a result, the SLA can operate within a wide frequency band. To reduce the height of the structure, one can truncate the top part as shown in Fig. 5(b). In this paper, a customized version of the truncated monopole SLA, compatible with multilayer PCB fabrication and integrated circuit technologies, is used to realize the described CP beamforming and steering method.

IV. ANTENNA DESIGN

Figure 6(a) shows the proposed truncated monopole SLA structure with the utilized PCB stack up. The PCB stack has 5 metal layers where layers 1-3 are made by 30 mil Rogers

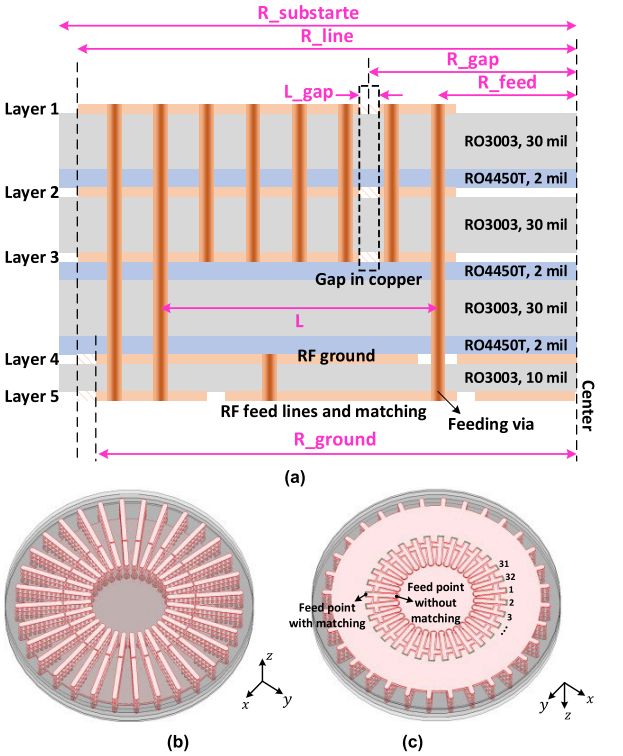

FIGURE 6. Antenna structure realizing the proposed beamforming and steering method. (a) Utilized PCB stack up and structure of the monopole SLA. (b) Top view of the antenna (modeled in HFSS) showing the lines and vias with the corresponding coordinate system. (c) Bottom view of the modeled antenna showing the feed points with and without matching circuit.

TABLE 1. Optimized geometrical parameters of the antenna.

R_substrate	13 mm	Through hole via diameter	0.318 mm
R_line	11.7 mm	Via diameter (Layer 1 to 3)	0.254 mm
R_ground	11 mm	Via diameter (Layer 4 to 5)	0.203 mm
R_gap	6.95 mm	Stub distance from feeding via	2.1 mm
R_feed	4.2 mm	Open stub length	0.86 mm
L_gap	0.127 mm	GCPW line width	0.432 mm
L	5 mm	GCPW line gap	0.127 mm

RO3003 materials (a low-loss high-frequency material with dielectric constant of 3). These layers are bonded together using Rogers RO4450T bond ply. The fourth layer is a ground plane serving as a ground for the monopole SLAs as well as the grounded coplanar waveguide (GCPW) feed lines at the bottom side of the antenna. The 10-mil RO3003 layer underneath the ground plane is for feed lines and matching. The geometrical parameters are indicated in Fig. 6(a). The radii of the ground planes on layers 4 and 5 are equal to R_ground.

The proposed truncated monopole SLAs are realized by the metal layers 1-3 and the vias connecting these layers. The short circuit at the end of each SLA is realized by through-hole vias connecting all layers particularly layer 1 to layer 4. To provide a feed for each SLA, a through-hole via is used to connect the layers 1-3. This via is also passed through the ground plane and is connected to layer 5 (GCPW lines). A total of 32 SLA elements are used to excite the first 8 TE_{n1} modes and their rotated copies. The antenna is modeled in

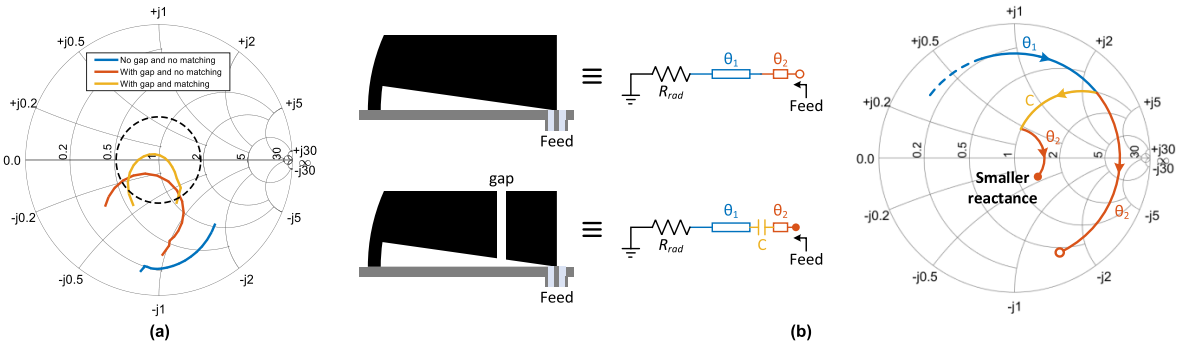

FIGURE 7. Impedance matching. (a) Complex reflection coefficient from one port while other ports are terminated to 50 Ω (from 26 GHz to 30 GHz). Dashed line shows reflection coefficient = 0.32 = -10 dB. (b) Equivalent circuits of the SLAs with and without gap, and the impact of the utilized gap (modelled with a series capacitor) on reducing the input reactance.

ANSYS HFSS as shown in Figs. 6(b) and (c) (top and bottom views, respectively). It should be emphasized that in the proposed beamforming and steering antenna, each TE_{n1} mode in conjunction with its rotated copy, not the individual SLA elements, acts like an antenna in a conventional phased array.

To design the antenna, first, R_feed is set to the minimum possible value to facilitate the fabrication process (smaller values of R_feed results in a smaller spacing between the feed points). Based on the analysis in Fig. 3, L + R_feed is initially set to $0.6\lambda_0$ (λ_0 is the free-space wavelength at the center frequency of operation, i.e., 28 GHz).

In the next step, the antenna geometry without any gap at the top or mid-layer coppers is optimized for AR $<$ 3 dB over the operation band (26.5-29.5 GHz) at each of the 8 modes. The resulting complex reflection coefficient for such an antenna is shown in Fig. 7(a). Here, the reflection coefficient is considered from one feed point (due to the symmetry, all feed points, indicated in Fig. 6(c), show the same response) while no matching circuit is present, and all other ports are terminated to 50 Ω. According to Fig. 7(a), the input impedance exhibits a large reactance which disrupts wideband matching. However, this series reactance can be reduced by realizing a series capacitor. Based on the geometry of the SLA element shown in Figs. 5(b) and 6(a), the SLA can be modeled as a resistor R_{rad} (modeling the radiation resistance), in series with a transmission line with an electrical length of $\theta_1 + \theta_2$ as illustrated in Fig 7(b). According to Fig. 7(b), by placing a series capacitor within the transmission line and close to the feed, the input reactance would be reduced. The required series capacitance can be realized by introducing a gap at the top and mid-layers as shown in Fig. 6(a) and Fig. 7(b). The gap length (L_gap) is set to 0.127 mm (= 5 mil) to satisfy the PCB fabrication requirements. The corresponding reflection coefficient, shown in Fig. 7(a), represents a lower input reactance. The resulting impedance can be decently matched to 50 Ω over a wide frequency band using a single stub at the bottom layer of the antenna, shown in Fig. 6(c) (the feed points are also shown). Fig. 7(a) also includes the input reflection coefficient (from one port) after using the described single stub matching network. As can be seen, the resulting reflection coefficient is less than -10 dB over a wide frequency band (26.5-29.5 GHz).

The optimized geometrical parameters of the antenna are listed in Table 1. To provide an RHCP (or LHCP) radiation, the excitations in (8) (or their complex conjugates) should be applied to the ports of the antenna in Figs. 6(b) and (c) whose numbering is increasing in $+\hat{\phi}$ direction. The circular structure of the antenna's feed points allows for a simpler routing of its feed network compared to linear phased arrays [28], [29], [30].

To provide the required excitations for the proposed 4N-port antenna, one can use an integrated beamformer with $4N$ channels, each including a vector modulator [31], at the center of the antenna's ground plane on layer 5. The vector modulators' outputs can be simply connected to the ports of the antenna with radial lines.

V. ANTENNA FABRICATION AND PERFORMANCE

The designed antenna with 32 ports has been fabricated, and its photograph is shown in Figs. 8(a) and (b). The antenna's diameter is 26 mm, and its total height excluding the connector is 2.8 mm.

The antenna structure is completely symmetric, and the fields radiated by a general port m is basically an azimuthal rotated copy of the fields radiated by port 1. The angle of rotation is equal to the azimuthal angle between the SLA elements connected to ports 1 and m. This property of the radiated fields is used for measurements, and only one port of the antenna is fed (by a high-frequency SMPM connector placed at the center of the antenna at layer 5) and measured while the other ports are terminated to 50 Ω (using high frequency resistors), as shown in Fig. 8(b). The configuration and geometry of the fabricated antenna are the same as Figs. 6(b) and (c) except that the feed line of the port under test is rotated so that the connector can be placed at the center of the antenna to avoid unwanted scatterings (by the connector and its attached cable). The antenna's performance has been measured in an anechoic chamber with the setup shown in Fig. 8(c).

The exact configuration of the fabricated antenna has also been modeled and simulated in Ansys HFSS. The top side of the model is shown in Fig. 6(b), and the bottom side with and without connector is shown in Fig. 8(d) and Fig. 6(c), respectively.

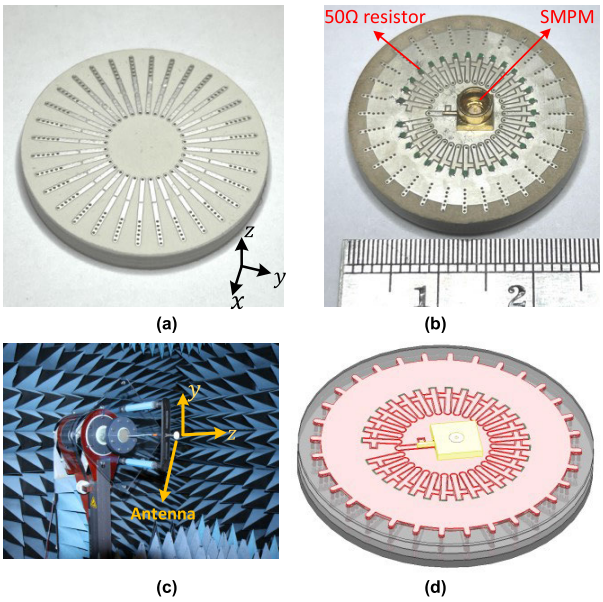

FIGURE 8. Fabricated antenna with one excited port. (a) Top view of the antenna. (b) Bottom view of the antenna. (c) Measurement setup in anechoic chamber. (d) HFSS model (bottom side) of the fabricated antenna with one feed (SMPM connector).

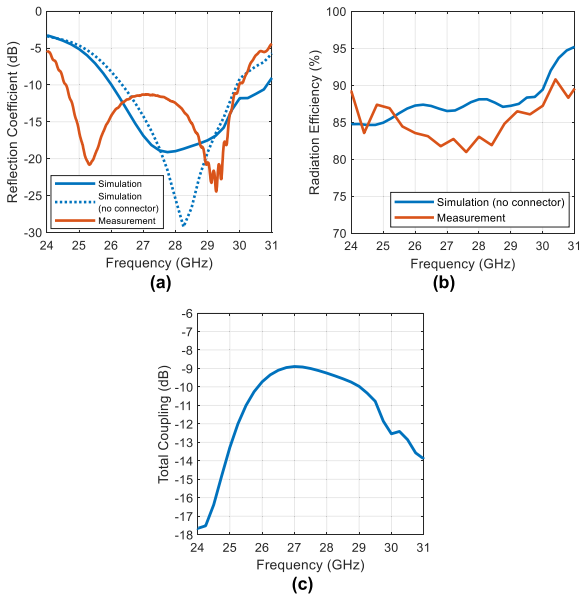

FIGURE 9. (a) Simulated and measured reflection coefficient for one port while the other ports are terminated to 50 Ω. (b) Simulated and measured radiation efficiency. Measured values are obtained by the measured total efficiency and simulated active S-parameters and directivity. (c) Simulated total coupling for the port of the antenna that exhibits the maximum coupling among all ports when the antenna is excited for CP beam steering with 8 modes.

Figure 9(a) shows the simulated (with and without connector) and measured reflection coefficients for the fabricated antenna. According to the simulation results, reflection coefficient is less than −10 dB within 26.25-30 GHz for the antenna without connector and is less than −10 dB within a wider frequency band for the antenna with connector. The discrepancy between simulation and measurement results is majorly due to the fabrication errors (particularly, the errors

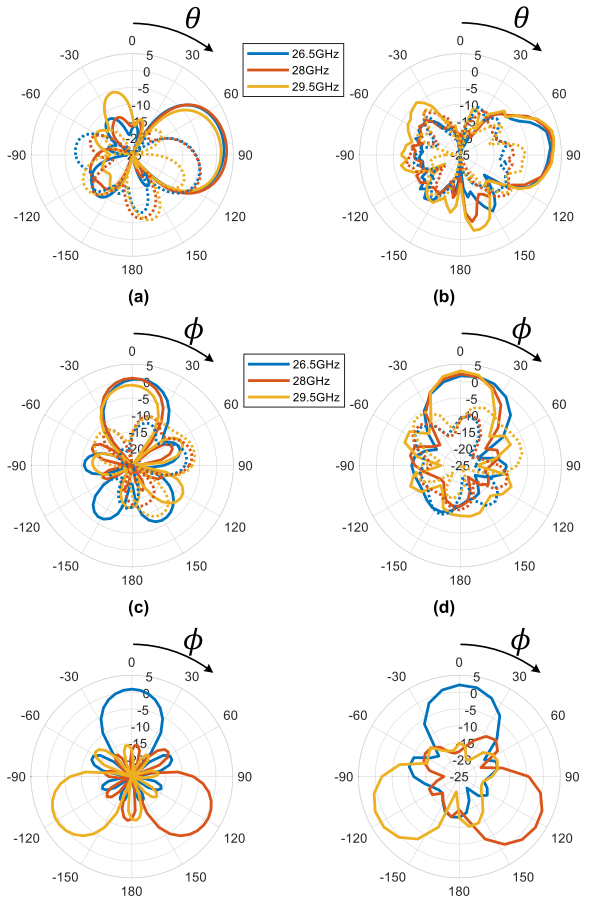

FIGURE 10. (a) Simulated and (b) measured realized RHCP (solid lines) and LHCP (dashed lines) gains over elevation at $\phi = 0°$ (while the beam is steered to $\phi_s = 0°$). (c) Simulated and (d) measured realized RHCP (solid lines) and LHCP (dashed lines) gains versus ϕ (while the beam is steered to $\phi_s = 0°$). (e) Simulated and (f) measured realized RHCP gains versus ϕ at 28 GHz while the beam is steered to $\phi_s = 0°$, 120°, and 240°. The coordinate system for the patterns is shown in Fig. 8(a).

in the thickness of bond ply layers within the PCB stack up). Figure 9(b) shows the antenna's radiation efficiency versus frequency, and based on the simulated and measured results, radiation efficiency is more than 80% from 26.5 to 29.5 GHz. Measured values are obtained by measured total efficiency and simulated active S-parameters and directivity. Figure 9(c) shows the simulated total coupling for the port of the antenna that exhibits the maximum coupling among all ports when the antenna is excited for CP beam steering with 8 modes. The total coupling is defined as the ratio of the total power coupled to the port from the other ports to the total input power to the other ports.

Figures 10(a) and (b) show the simulated and measured realized CP gain patterns over elevation at $\phi = 0°$, respectively. The results are obtained for the described antenna excited to direct its beam to $\phi_s = 0°$. Based on the gain patterns, shown at 26.5, 28, and 29.5 GHz, radiation is directive and RHCP for the entire cases. Figures 10(c) and (d), respectively, show the simulated and measured realized gain patterns over azimuth for the antenna excited to direct its

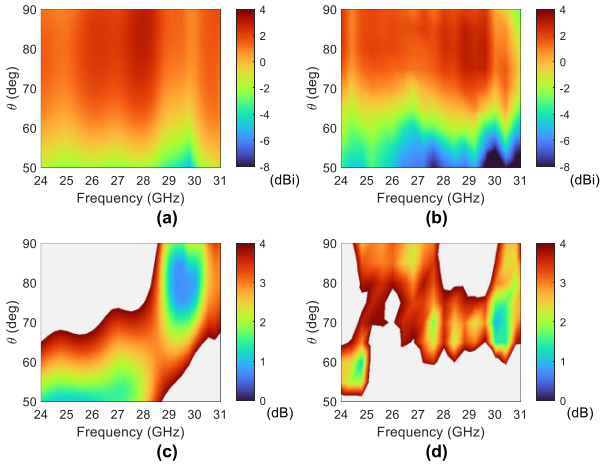

FIGURE 11. (a) Simulated and (b) measured realized RHCP gain versus frequency and θ at $\phi = 0°$ while the RHCP beam is steered to $\phi_s = 0°$. (c) Simulated and (d) measured AR versus frequency and θ at $\phi = 0°$ while the RHCP beam is steered to $\phi_s = 0°$ (the gray color indicates values larger than 4 dB). The coordinate system is shown in Fig. 8(a).

beam to $\phi_s = 0°$. As can be observed, radiation is RHCP while directed to $\phi = 0°$. The sidelobe levels at 26.5 GHz, 28 GHz, and 29.5 GHz are, respectively, −7.2 dB, −13 dB, and −6.5 dB for simulation results and −11.8 dB, −11.9 dB, and -9.9 dB for measurement results. Figures 10(e) and (f), respectively, show the simulated and measured realized RHCP gain patterns over azimuth for the beam steered to $\phi_s = 0°$, 120°, and 240°. The results, given at 28 GHz, verify that the features of radiation pattern do not change with beam steering.

Figures 11(a) and (b) show, respectively, the simulated and measured realized RHCP gain of the antenna as a function of frequency and θ at $\phi = 0°$, with the beam steered to $\phi_s = 0°$. The maximum realized RHCP gain is 3 dBi for both simulations and measurements. Figures 11(c) and (d) also show, respectively, the simulated and measured AR of the antenna versus frequency and θ at $\phi = 0°$ while the beam is stered to $\phi_s = 0°$. As per the simulation results presented in Fig. 11(c), the antenna shows a CP performance (AR < 3 dB) over the entire band of interest (26.5-29.5 GHz). However, the CP beam is tilted to a larger θ as the frequency increases. According to the measured results, in Fig. 11(d), the measured AR is also less than 3.5 dB within 26.5-29.5 GHz. The difference between the simulated and measured AR is primarily attributed to the variations in the thickness of the dielectric layers (specifically prepreg layers), deviating from the originally designed values.

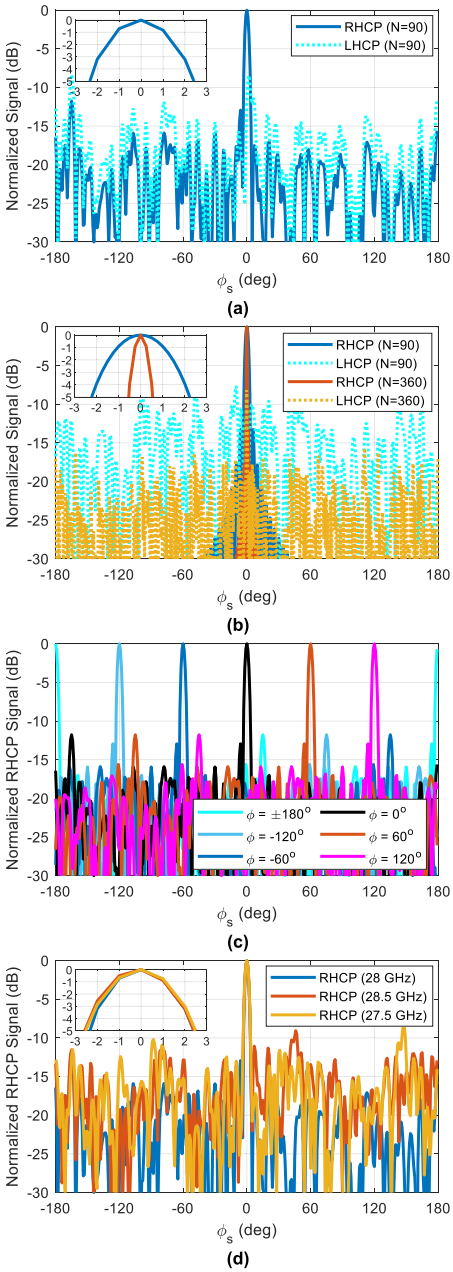

FIGURE 12. Simulated and measured results showing the CP signals received from an RHCP source located at an azimuthal angle of ϕ versus steering angle (ϕ_s) while the beam is synthesized with N modes and steered over azimuth. (a) Measured results obtained for a 28-GHz RHCP source at $\phi = 0°$ with $N = 90$ synthesized modes. (b) Simulated results for a 28-GHz RHCP source at $\phi = 0°$ with $N = 90$ and 360 synthesized modes. (c) Simulated results for a 28-GHz RHCP source at different azimuthal angles ϕ, using $N = 90$ synthesized modes. (d) Simulated results for an RHCP source at $\phi = 0°$ and at different frequencies of 27.5, 28, 28.5 GHz with $N = 90$ synthesized modes.

VI. SYNTHESIS OF THE PROPOSED BEAMFORMING AND STEERING METHOD FOR HIGH ANGULAR RESOLUTION 360° COVERAGE RADAR APPLICATIONS

According to (5), if N modes are uniformly excited ($a_n = 1$), the 3-dB beamwidth (in radians) of the proposed beamforming method is approximately $2(\pi/N)$. Thus, to achieve an angular resolution of, for example 2°, 180 modes should be excited, requiring 720 elements. However, using so many elements is impractical. Instead, one can achieve the desired functionality by using just one rotating SLA element on a circular ground plane. This simple structure with only one feed point can provide a high angular resolution using the proposed method, as detailed below.

Assuming an SLA element, initially located at an azimuthal angle of $\phi = 0°$, rotates in azimuth from 0° to 360°;

the signals received at M equally spaced azimuthal angles, $\phi_m = (m\text{-}1)\times 360°/M$ ($m = 1, 2, 3, \ldots, M$), are given by the vector

$$E_1 = \left[e_1 \; e_2 \; e_3 \; \cdots \; e_{M-2} \; e_{M-1} \; e_M \right], \tag{10}$$

where e_m is the complex signal measured at ϕ_m. As discussed in Section V, in the proposed antenna featuring multiple SLAs in circular symmetry, the signal received by the mth SLA over azimuth is a rotated copy of the signal received by the first SLA. The rotation angle is equal to the angular spacing between the first and the mth element. Thus, if the vector of signals received by a real rotating SLA, initially located at $\phi = 0°$, is represented as E_1 (10), then the vector of the signals received by a virtual rotating SLA, initially located at ϕ_m (denoted as E_m), would be identical to E_1 with its elements circularly shifted by $m-1$. As several examples, E_2, E_3, and E_M, are given by

$$E_2 = \left[e_2 \; e_3 \; e_4 \; \cdots \; e_{M-1} \; e_M \; e_1 \right]. \tag{11a}$$

$$E_3 = \left[e_3 \; e_4 \; e_5 \; \cdots \; e_M \; e_1 \; e_2 \right]. \tag{11b}$$

$$E_M = \left[e_M \; e_1 \; e_2 \; \cdots \; e_{M-3} \; e_{M-2} \; e_{M-1} \right]. \tag{11c}$$

Thus, by measuring the signals received by a single rotating SLA at M azimuthal angles, the signals received by M virtual rotating SLAs can be obtained. In this scenario, combining these signals, denoted as E_m ($m = 1, 2, 3, \ldots, M$), using the coefficients described by (8), provides a beamwidth equivalent to exciting the first $N = M/4$ modes. Combination of the signals using the described method results in a high processing gain similar to synthetic aperture radar (SAR). For beam steering purposes, ϕ_s should be adjusted in (8).

As proof of concept, a single active SLA antenna is rotated, and the signals it receives from an RHCP source located at an azimuthal angle of ϕ are captured at 360 (and 1440) equally spaced angles over azimuth. Utilizing the collected data, it becomes possible to synthesize the described CP beamforming and steering method with N reaching up to 90 (and 360) modes. Figure 12 shows the normalized RHCP and LHCP signals received as the beam is synthesized and steered over azimuth for $N = 90$ (and 360).

Figure 12(a) shows the measured CP signals received from a 28-GHz RHCP source at $\phi = 0°$, plotted versus steering angle (ϕ_s), while the beam is synthesized with $N = 90$ modes and steered over azimuth. The peak of the RHCP signal is observed at $\phi = 0°$ (where the source is located) with a 3-dB beamwidth (resolution) of 4°. There is also a 9 dB difference between RHCP and LHCP signals at $\phi = 0°$.

Figure 12(b) shows the simulated CP signals received from a 28-GHz RHCP source at $\phi = 0°$ as a function of ϕ_s. Figure 12(b) is obtained while the beam is synthesized with $N = 90$ and 360 modes and steered over azimuth. It can be observed that the peak of the RHCP signal occurs at $\phi_s = 0°$; and the beamwidth becomes narrower as N increases.

Figure 12(c) shows the simulated received RHCP signal at 28 GHz versus ϕ_s while the beam is synthesized with $N = 90$ modes and steered over azimuth in presence of an RHCP source at different azimuthal angles ϕ. As expected, the resolution remains constant as the source azimuthal angle varies.

In Fig. 12(d), simulated received RHCP signals at frequencies of 27.5 GHz, 28 GHz, and 28.5 GHz are plotted versus ϕ_s while the beam is synthesized with $N = 90$ modes and steered over azimuth in the presence of an RHCP source at $\phi = 0°$. In Figs. 12(a)-(d), c_n's in (8) are derived at 28 GHz. Notably, the antenna demonstrates an operational bandwidth of at least 1 GHz centered at 28 GHz.

The described technique can be applied to 77-GHz band to achieve LIDAR-like resolution with full 360° coverage in automotive applications while maintaining the advantages of radar systems (functionality in severe weather conditions).

VII. CONCLUSION

A new beamforming and steering technique that allows a 360° spatial coverage with a compact antenna has been proposed. This technique is based on utilizing a plurality of superposed circular TE_{n1} modes. It has been theoretically shown that each TE_{n1} mode in conjunction with its rotated copy provides an omnidirectional CP radiation with a unique spatial phase profile. This phase profile has been leveraged to accomplish beamforming and steering. A new low-profile antenna structure realizing the introduced method within 5G bands has also been proposed. This antenna has been designed and fabricated, and the simulation and measurement results have been presented and discussed.

The advantages of the described beamforming and steering technique and its realizing antenna are as follows: a) 360° beam steering can be accomplished using a single low-profile compact antenna; b) the pattern shape remains constant as the beam is steered; c) there is no missing angular coverage range in this method; d) the antenna has a small lateral dimension compared to available CP phased array antennas with 360° coverage, which makes the described design suitable for integration with user equipment; e) the antenna structure is compatible with integrated circuit technology, allowing for its use as an on-chip antenna; f) the antenna provides a CP directive radiation over a wide frequency band, which is beneficial for mm-wave communications; g) the handedness of the circular polarization is independent of the antenna's physical structure and is set by the phase/amplitude of excitations; h) the antenna's CP radiation pattern can be easily switched between an omnidirectional pattern or a steerable directional pattern by changing only the excitations' phases and amplitudes; i) the antenna's structure allows for a simple routing of the required feeds.

It has also been demonstrated that the method can be implemented using a small rotating antenna to provide a very high angular resolution for radar applications.

REFERENCES

[1] B. Coll-Perales, M. C. Lucas-Estañ, T. Shimizu, J. Gozalvez, T. Higuchi, S. Avedisov, O. Altintas, and M. Sepulcre, "End-to-end V2X latency modeling and analysis in 5G networks," *IEEE Trans. Veh. Technol.*, vol. 72, no. 4, pp. 5094–5109, Apr. 2023.

[2] J. Kim, Y.-J. Choi, G. Noh, and H. Chung, "On the feasibility of remote driving applications over mmWave 5G vehicular communications: Implementation and demonstration," *IEEE Trans. Veh. Technol.*, vol. 72, no. 2, pp. 2009–2023, Feb. 2023.

[3] M. Jafri, S. Srivastava, S. Anwer, and A. K. Jagannatham, "Sparse parameter estimation and imaging in mmWave MIMO radar systems with multiple stationary and mobile targets," *IEEE Access*, vol. 10, pp. 132836–132852, 2022.

[4] A. I. Sulyman, A. T. Nassar, M. K. Samimi, G. R. Maccartney, T. S. Rappaport, and A. Alsanie, "Radio propagation path loss models for 5G cellular networks in the 28 GHZ and 38 GHZ millimeter-wave bands," *IEEE Commun. Mag.*, vol. 52, no. 9, pp. 78–86, Sep. 2014.

[5] M. Jafri, A. Anand, S. Srivastava, A. K. Jagannatham, and L. Hanzo, "Robust distributed hybrid beamforming in coordinated multi-user multi-cell mmWave MIMO systems relying on imperfect CSI," *IEEE Trans. Commun.*, vol. 70, no. 12, pp. 8123–8137, Dec. 2022.

[6] R. Hussain and M. S. Sharawi, "5G MIMO antenna designs for base station and user equipment: Some recent developments and trends," *IEEE Antennas Propag. Mag.*, vol. 64, no. 3, pp. 95–107, Jun. 2022.

[7] J. Zhu, Y. Yang, S. Li, S. Liao, and Q. Xue, "Dual-band dual circularly polarized antenna array using FSS-integrated polarization rotation AMC ground for vehicle satellite communications," *IEEE Trans. Veh. Technol.*, vol. 68, no. 11, pp. 10742–10751, Nov. 2019.

[8] Y.-F. Cheng, Y.-X. Wang, J.-L. Zhong, C. Liao, and X. Ding, "Shared-metasurface antenna with diverse reflection, radiation and polarization characteristics for vehicular communications," *IEEE Trans. Veh. Technol.*, vol. 72, no. 6, pp. 7573–7583, Jun. 2023.

[9] M. Nouri, H. Behroozi, A. Jafarieh, S. A. Aghdam, J. Piran, and N. K. Mallat, "A learning-based dipole yagi-uda antenna and phased array antenna for mmWave precoding and V2V communication in 5G systems," *IEEE Trans. Veh. Technol.*, vol. 72, no. 3, pp. 2789–2803, Mar. 2023.

[10] A. M. A. Najafabadi, F. A. Ghani, and I. Tekin, "Low-cost multibeam millimeter-wave array antennas for 5G mobile applications," *IEEE Trans. Veh. Technol.*, vol. 71, no. 12, pp. 12450–12460, Dec. 2022.

[11] H. Ozpinar, S. Aksimsek, and N. T. Tokan, "A novel compact, broadband, high gain millimeter-wave antenna for 5G beam steering applications," *IEEE Trans. Veh. Technol.*, vol. 69, no. 3, pp. 2389–2397, Mar. 2020.

[12] J.-Y. Lee, J. Choi, D. Choi, Y. Youn, and W. Hong, "Broadband and wide-angle scanning capability in low-coupled mm-wave phased-arrays incorporating ILA with HIS fabricated on FR-4 PCB," *IEEE Trans. Veh. Technol.*, vol. 70, no. 3, pp. 2076–2088, Mar. 2021.

[13] K. Chen, J. Xu, Q. Lin, Y. Zhu, and W. Hong, "Single-layer wideband tilted beam phased array antenna for millimeter-wave vehicle communications," *IEEE Trans. Veh. Technol.*, vol. 73, no. 3, pp. 3536–3550, Mar. 2024.

[14] Q. Wu, J. Hirokawa, J. Yin, C. Yu, H. Wang, and W. Hong, "Millimeter-wave multibeam endfire dual-circularly polarized antenna array for 5G wireless applications," *IEEE Trans. Antennas Propag.*, vol. 66, no. 9, pp. 4930–4935, Sep. 2018.

[15] S. Sadeghi-Marasht, M. S. Sharawi, and A. Zhu, "Dual-band circularly polarized antenna array for 5G millimeter-wave applications," *IEEE Open J. Antennas Propag.*, vol. 3, pp. 314–323, 2022.

[16] K. R. Mahmoud and A. M. Montaser, "Design of dual-band circularly polarised array antenna package for 5G mobile terminals with beam-steering capabilities," *IET Microw., Antennas Propag.*, vol. 12, no. 1, pp. 29–39, Jan. 2018.

[17] N. J. G. Fonseca, "Design and implementation of a closed cylindrical BFN-fed circular array antenna for multiple-beam coverage in Azimuth," *IEEE Trans. Antennas Propag.*, vol. 60, no. 2, pp. 863–869, Feb. 2012.

[18] M. C. Derbal and M. Nedil, "High-gain circularly polarized antenna array for full incident angle coverage in RF energy harvesting," *IEEE Access*, vol. 11, pp. 28199–28207, 2023.

[19] F. Akbar and B. Yektakhah, "360° beam steering with circular polarization based on the superposition of circular TE_{n1} modes," in *Proc. IEEE Int. Symp. Antennas Propag. USNC-URSI Radio Sci. Meeting (APS/URSI)*, Singapore, Dec. 2021, pp. 503–504.

[20] Y. M. Pan, S. Y. Zheng, and B. J. Hu, "Wideband and low-profile omni-directional circularly polarized patch antenna," *IEEE Trans. Antennas Propag.*, vol. 62, no. 8, pp. 4347–4351, Aug. 2014.

[21] B.-C. Park and J.-H. Lee, "Omnidirectional circularly polarized antenna utilizing zeroth-order resonance of epsilon negative transmission line," *IEEE Trans. Antennas Propag.*, vol. 59, no. 7, pp. 2717–2721, Jul. 2011.

[22] W. Lin and H. Wong, "Circularly polarized conical-beam antenna with wide bandwidth and low profile," *IEEE Trans. Antennas Propag.*, vol. 62, no. 12, pp. 5974–5982, Dec. 2014.

[23] Y. Shi and J. Liu, "Wideband and low-profile omnidirectional circularly polarized antenna with slits and shorting-vias," *IEEE Antennas Wireless Propag. Lett.*, vol. 15, pp. 686–689, 2016.

[24] A. Li and K.-M. Luk, "Single-layer wideband end-fire dual-polarized antenna array for device-to-device communication in 5G wireless systems," *IEEE Trans. Veh. Technol.*, vol. 69, no. 5, pp. 5142–5150, May 2020.

[25] M. M. Samadi Taheri, A. Abdipour, S. Zhang, and G. F. Pedersen, "Integrated millimeter-wave wideband end-fire 5G beam steerable array and low-frequency 4G LTE antenna in mobile terminals," *IEEE Trans. Veh. Technol.*, vol. 68, no. 4, pp. 4042–4046, Apr. 2019.

[26] H. Cho, J.-H. Lee, J.-W. Yu, and B. Ahn, "Series-fed coupled split-ring resonator array antenna with wide fan-beam and low sidelobe level for millimeter-wave automotive radar," *IEEE Trans. Veh. Technol.*, vol. 72, no. 4, pp. 4805–4814, Apr. 2023.

[27] N. Behdad and K. Sarabandi, "A compact antenna for ultrawideband applications," *IEEE Trans. Antennas Propag.*, vol. 53, no. 7, pp. 2185–2192, Jul. 2005.

[28] F. Akbar and A. Mortazawi, "A K-band low-complexity modular scalable wide-scan phased array," in *IEEE MTT-S Int. Microw. Symp. Dig.*, Los Angeles, CA, USA, Aug. 2020, pp. 1227–1230.

[29] F. Akbar and A. Mortazawi, "Scalable phased array architectures with a reduced number of tunable phase shifters," *IEEE Trans. Microw. Theory Techn.*, vol. 65, no. 9, pp. 3428–3434, Sep. 2017.

[30] F. Akbar and A. Mortazawi, "Design of a scalable phased array antenna with a simplified architecture," in *Proc. Eur. Microw. Conf. (EuMC)*, Paris, France, Sep. 2015, pp. 1427–1430.

[31] F. Akbar and A. Mortazawi, "A frequency tunable 360° analog CMOS phase shifter with an adjustable amplitude," *IEEE Trans. Circuits Syst. II, Exp. Briefs*, vol. 64, no. 12, pp. 1427–1431, Dec. 2017.

FATEMEH AKBAR (Member, IEEE) received the Ph.D. degree in electrical engineering from the University of Michigan, Ann Arbor, USA, in 2018.

Afterwards, she joined California Institute of Technology (Caltech), as a Postdoctoral Research Scholar. She is currently an Assistant Professor with the Department of Electrical Engineering, Sharif University of Technology. Her research interests include wireless and wireline communication systems, radars, RF/mm-wave IC design, ultra-low-power IC design, bioelectronics, and applied electromagnetics.

Ms. Akbar received the Engineering Graduate Symposium Technical Award from the University of Michigan's College of Engineering, in 2014, 2016, and 2017. She was also named as a Rising Star by MIT's EECS, in 2018; and was selected as an Excellent Graduate Student Instructor by the Department of Electrical Engineering and Computer Science, University of Michigan, in Winter 2018.

BEHZAD YEKTAKHAH (Member, IEEE) received the B.S. and M.S. degrees in electrical engineering from the University of Tehran, Tehran, Iran, in 2008 and 2011, respectively, and the Ph.D. degree in electrical engineering from the University of Michigan, Ann Arbor, in 2019.

His research interests include applied electromagnetics, signal processing, radar and communication systems, wave propagation and scattering, antennas, and phased arrays.